Applied Catalysis B: Environmental 140–141 (2013) 199–205

Contents lists available at SciVerse ScienceDirect

Applied Catalysis B: Environmental

journal homepage: www.elsevier.com/locate/apcatb

# Enhanced performance in catalytic combustion of toluene over mesoporous Beta zeolite-supported platinum catalyst

Chunyu Chen[a], Jie Zhu[a], Fang Chen[a], Xiangju Meng[a,*], Xiaoming Zheng[a], Xionghou Gao[b], Feng-Shou Xiao[a,c,**]

[a] Key Lab of Applied Chemistry of Zhejiang Province, Department of Chemistry (Xixi Campus), Zhejiang University, Hangzhou 310028, China
[b] Lanzhou Petrochemical Research Center, Petrochemical Research Institute, Petro China Company Limited, Lanzhou 730060, China
[c] Zhejiang Provincial Engineering Research Center of Industrial Boiler & Furnace Flue Gas Pollution Control, Hangzhou 310027, China

ARTICLE INFO

*Article history:*
Received 29 January 2013
Received in revised form 16 March 2013
Accepted 29 March 2013
Available online 6 April 2013

*Keywords:*
Mesoporous Beta zeolite
Supported platinum catalyst
Catalytic combustion
Volatile organic compounds (VOCs)
Toluene

ABSTRACT

Removal of volatile organic compounds (VOCs) has recently been attracted much attention, and catalytic combustion is one of good methods for solving this problem. In this research, we show a successful preparation of mesoporous Beta zeolite-supported Pt catalyst (Pt–R/Beta-H) and its superior performance in the catalytic combustion of toluene. $N_2$ sorption isotherms show that the mesopore volume of Pt–R/Beta-H reaches 0.18 $cm^3/g$, and TEM images exhibit that the Pt particles exist in both micropores and mesopores of the sample. Interestingly, the Pt particles on Pt–R/Beta-H have higher dispersion than the Pt particles on conventional Beta zeolite (Pt–R/Beta). XPS spectra also reveal that Pt–R/Beta-H has higher $Pt^0/Pt^{2+}$ ratio than Pt–R/Beta. Very importantly, Pt–R/Beta-H exhibits much higher catalytic activities and longer catalyst life as well as lower apparent activation energy in the catalytic combustion of toluene than Pt–R/Beta. The extraordinary performance in the catalytic combustion of toluene over Pt–R/Beta-H catalyst is of great importance for obtaining clean environment and enhancing human health.



## 1. Introduction

Volatile organic compounds (VOCs) are the major components of air pollutants from motor vehicles and industrial processes as well as domestic products. Most of VOCs are precursors of ozone and photochemical smog, which are great threats to the environment and human health because of their toxic, carcinogenic, mutagenic, and teratogenetic nature [1–3]. Thus, elimination of VOCs has become one of hot research topics, due to safe concerns together with more stringent legislations [2,4]. Up to now, a series of techniques for removing VOCs have been well developed, such as adsorption, thermal incineration, photocatalytic degradation, plasma catalytic oxidation, and catalytic combustion. Among these techniques, catalytic combustion has been identified as one of the most effective, economically feasible, and promising routes for VOCs abatement, especially for low concentration VOCs at much lower temperature [5–7].

Perovskites [8], transition metal oxides [9], and supported noble metals [10–16] are the most used catalysts for the catalytic combustion of VOCs, due to their excellent activities, high thermal stabilities, and high resistance to deactivation. Generally, zeolites, alumina, zirconia, titania, and silica have been extensively applied as supports for preparation of supported noble metal catalysts [10–16]. For example, Becker and Förster investigated oxidative decomposition of benzene and its methyl derivatives over NaY, CuY, PdHY, and PdY zeolites [17,18], and they found that PdY was the most active catalyst. Siffert and co-workers compared FAU zeolite, $ZrO_2$, and hierarchical macro-mesoporous $ZrO_2$ impregnated with 0.5% Pd for toluene total oxidation [19,20], and they observed that Pd/FAU zeolite gave better activity than Pd supported on macro-mesoporous $ZrO_2$ and conventional $ZrO_2$. Therefore, zeolite supports have recently been paid much attention in the catalytic combustion of VOCs, due to their large surface area, uniform and intricate channels, high adsorption capacity, acidic property, high thermal and hydrothermal stabilities [21–26]. However, the relatively small and sole micropores in conventional zeolites significantly influence the mass transfer in catalytic reactions, resulting in relatively easy coke formation and deactivation of catalysts [27–29]. For example, Magnoux et al. carefully investigated the coke formation within the pores of zeolite in the catalytic oxidation of *o*-xylene into $CO_2$ and $H_2O$ [30–32]. To solve the limitation of the zeolitic micropores, the use of mesoporous zeolites as the catalyst supports is strongly desirable.

Thanks for the great efforts of materials scientists, mesoporous zeolites with good mass transfer have been successfully

* Corresponding author.
** Corresponding author. Tel.: +86 57188273282.
*E-mail addresses:* mengxj@zju.edu.cn (X. Meng), fsxiao@zju.edu.cn (F.-S. Xiao).

0926-3373/$ – see front matter © 2013 Elsevier B.V. All rights reserved.
http://dx.doi.org/10.1016/j.apcatb.2013.03.050

synthesized recently, which combine the advantages of both mesoporous materials and zeolites [33–46]. However, to the best of our knowledge, the applications of mesoporous zeolites in the VOCs catalytic combustion have not been reported yet. Here, we demonstrate that mesoporous Beta (Beta-H) zeolite-supported Pt catalyst has high activities and superior catalyst life as well as low apparent activation energy in the catalytic combustion of low concentration toluene, compared with conventional Beta zeolite-supported Pt catalyst.

## 2. Experimental

### 2.1. Materials

Conventional Beta zeolite was supplied by Sinopec. NaOH (AR) and $NaAlO_2$ (CP) were purchased from Sinopharm Chemical Reagent Co., Ltd. Tetraethylammonium hydroxide (TEAOH, 25 wt%) and $H_2PtCl_6{\cdot}6H_2O$ (AR) were purchased from Aladdin. Fumed silica ($SiO_2$) was purchased from Shengyang Chemical Co., Ltd. Polydiallyldimethylammonium chloride (PDADMAC, 20 wt%, molecular weight of $\sim 1.5 \times 10^5$) was purchased from Yinhu Chemical Reagent Co., Ltd. $NH_4NO_3$ was purchased from Kelong Chemical Reagent Plant. Toluene (AR) was purchased from Hangzhou Chemical Reagent Co., Ltd.

### 2.2. Catalyst preparation

Mesoporous Beta zeolite (Beta-H) was synthesized according to the literature [33]. In a typical synthesis of Beta-H: NaOH (0.16 g) and $NaAlO_2$ (0.30 g) were mixed with TEAOH (32 mL), followed by addition of fumed silica (4.8 g). After stirring for 1 h at room temperature, PDADMAC (1.6 g) was added into the mixture. After stirring for 10–24 h at room temperature, the mixture was transferred into an autoclave at 140 °C for 120–240 h for crystallization. The product was collected by filtration, dried in air, and calcined at 550 °C for 5 h to remove the organic templates.

The H-form of Beta zeolite samples were ion-exchanged twice with a $NH_4NO_3$ solution (1 M) at 80 °C for 3 h, followed by calcination at 550 °C for 5 h.

Zeolite-supported Pt (1 wt%) catalysts were prepared by incipient wetness impregnation method using an appropriate amounts of aqueous solution of $H_2PtCl_6{\cdot}6H_2O$. The samples were then calcined at 550 °C for 5 h under dry air flow. These calcined Beta-H and Beta supported Pt catalysts were denoted as Pt–O/Beta-H and Pt–O/Beta. After reduction of Pt–O/Beta-H and Pt–O/Beta under 5% $H_2$/Ar flow (100 mL/min) at 500 °C for 2 h, the catalysts were denoted as Pt–R/Beta-H and Pt–R/Beta.

### 2.3. Catalyst characterization

X-ray diffraction (XRD) patterns were obtained with a RIGAKU Ultimate IV diffractometer using Cu Kα radiation. Nitrogen sorption isotherms at −196 °C were measured using a Micromeritics ASAP 2020M system. The surface area was calculated by using the Brunauer–Emmett–Teller (BET) method. The Si/Al ratios of the samples were determined by inductively coupled plasma (ICP) with a Perkin-Elmer plasma 40 emission spectrometer. The acidity of the samples was determined using the stepwise temperature-programmed desorption of ammonia automated chemisorption analysis unit ($NH_3$-TPD) with a thermal conductivity detector (TCD) under nitrogen flow. X-ray photoelectron spectra (XPS) of the samples were recorded using a Thermo ESCALAB 250 with Al Kα X-ray radiation for the X-ray source. The binding energies (BEs) were calibrated against Si2p (103.5 eV), Al2p (73.9 eV), and C1s (285.0 eV) peaks. Thermal gravimetric analysis (TGA) experiments were performed on a SDT Q600 V8.2 Build100 thermogravimetric analyzer. The scanning electron microscopy (SEM) images of the samples were recorded on a Hitachi SU 1510 apparatus. Transmission electron microscopy (TEM) experiments were performed on a JEM-3010 electron microscope (JEOL, Japan) with an acceleration voltage of 110 kV.

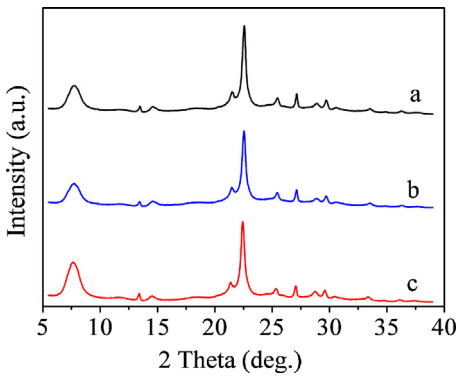


**Fig. 1.** XRD patterns of (a) Beta-H, (b) Pt–O/Beta-H, and (c) Pt–R/Beta-H samples.

### 2.4. Catalytic evaluation

The catalytic combustion of toluene experiments were performed in a continuous flow fixed-bed microreactor at the atmospheric pressure and temperatures between 100 and 240 °C, consisting of a quartz tube (6 mm i.d.) that was filled with the catalyst. A typical experiment was performed using a catalytic bed of 100 mg of catalyst (0.45–0.90 mm size) and with total flow rate of feed stream at 100 mL/min, giving a space velocity (SV) at 60,000 mL/(g h). The feed gas containing 1000 ppm toluene was generated by bubbling standard air (79% $N_2$ + 21% $O_2$) through a bottle containing pure toluene chilled in an ice-water isothermal bath, and then further diluted with another standard air stream before reaching the reaction bed. The concentrations of the toluene and oxidative products in the tail gas were analyzed by a gas chromatography (Kexiao, GC1690) equipped with a flame ionization detector (FID) using a 19091N-113 INNOWAX capillary column (Agilent, 30 m × 0.32 mm × 0.25 μm) for toluene, and a gas chromatography (Kexiao, GC1690) equipped with a thermal conductivity detector (TCD) using a Carboxen packed column (JieDao, 2 m × 2 mm) for $CO_2$ and CO.

The conversion of toluene was obtained based on toluene consumption, calculated by the inlet and outlet concentration of toluene. The selectivity to $CO_2$ was calculated by toluene consumption and outlet concentration of $CO_2$. The selectivity to side products was calculated by subtracting the selectivity to $CO_2$ from one. The catalytic activities were evaluated by the values of $T_5$, $T_{50}$, and $T_{98}$, which were defined as the temperatures at 5%, 50%, and 98% of toluene conversion, respectively.

## 3. Results and discussion

### 3.1. Catalyst characterization

Fig. 1 shows the XRD patterns of Beta-H, Pt–O/Beta-H, and Pt–R/Beta-H samples, exhibiting well-resolved characteristic peaks associated with Beta zeolite structure. These results suggest that these samples are basically stable during the impregnation, calcination, and reduction. Fig. 2 shows the nitrogen sorption isotherms of Beta-H, Pt–O/Beta-H, and Pt–R/Beta-H samples, giving a step at a relative pressure ($P/P_0$) of 0.4–0.95, which indicates the presence of mesoporosity in the samples. Correspondingly, these samples show BET surface areas and pore volumes at 432–483 $m^2$/g and

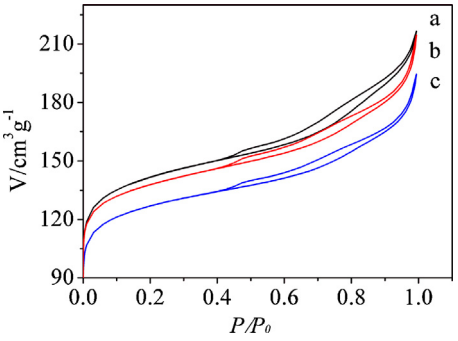


**Fig. 2.** Nitrogen sorption isotherms of (a) Beta-H, (b) Pt–R/Beta-H, and (c) Pt–O/Beta-H samples.

0.30–0.34 $cm^3/g$, as summarized in Table S1. Notably, after loading of Pt particles, the BET surface area and mesopore volume were slightly reduced. This phenomenon could be reasonably assigned to the presence of Pt particles in zeolite pores. Additionally, the Si/Al ratios of Beta (12.1) and Beta-H (12.9) are similar, exhibiting similar acidity (Fig. S1).

Fig. 3 shows the TEM images and Pt particle size distribution of Pt–R/Beta-H and Pt–R/Beta samples, exhibiting direct evidence for the presence of Pt nanoparticles. Notably, the Pt particle sizes ($1.8 \pm 0.6$ nm, Fig. 3A-a and B-a) on Pt–R/Beta-H are obviously smaller than those ($2.4 \pm 0.8$ nm, Fig. 3A-b and B-b) on Pt–R/Beta, indicating that the presence of mesoporosity in Pt–R/Beta-H is very favorable for high dispersion of Pt particles in the zeolite support. Moreover, high magnification TEM image clearly shows the mesopores in Pt–R/Beta-H sample (Fig. 4 and Fig. S2), and Pt particles can be found in these mesopores (Fig. 3 and Fig. S3A). Particularly, very small Pt particles can be observed in the micropores (Fig. 4 and Fig. S3B), which is possibly assigned to the confined effect of micropores [47,48].

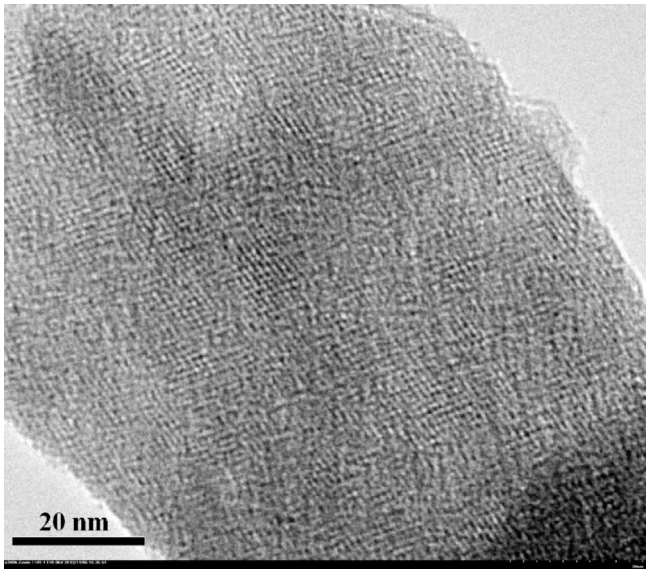


**Fig. 4.** High magnification TEM image of Pt–R/Beta-H.

Fig. 5 shows the Pt4f XPS spectra of Pt–R/Beta-H, Pt–O/Beta-H, Pt–R/Beta, and Pt–O/Beta samples. Since the Al2p peak strongly overlaps with the Pt4f peak in the range of 68–80 eV, it is necessary to separate the Al2p peak from the spectra. In our case, the Al2p is used at 73.9 eV, the $Pt4f_{7/2}$ spectra could be deconvoluted into two peaks at 70.1 together with 71.0 eV, and the $Pt4f_{5/2}$ spectra could be also deconvoluted into two peaks at 73.4 together with 74.3 eV associated with $Pt^0$ and $Pt^{2+}$, which are well consistent with those

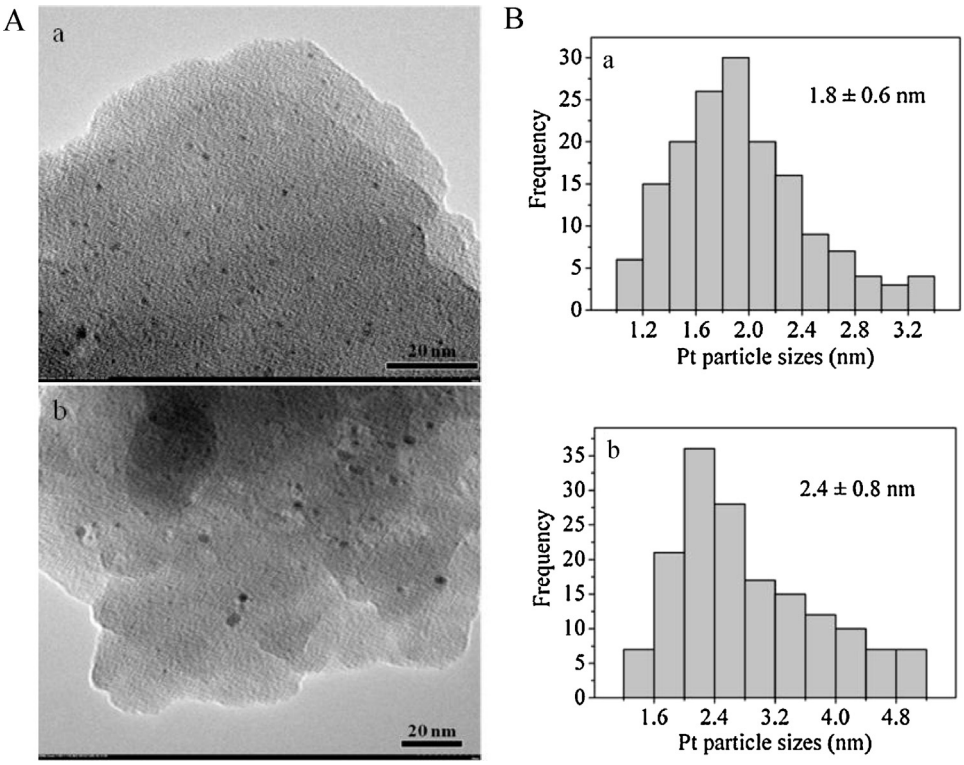


**Fig. 3.** (A) TEM images and (B) Pt particle size distribution of (a) Pt–R/Beta-H and (b) Pt–R/Beta samples.

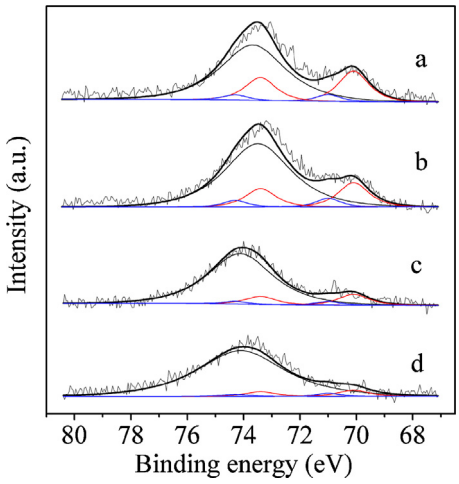


**Fig. 5.** Pt4f XPS spectra of (a) Pt–R/Beta-H, (b) Pt–O/Beta-H, (c) Pt–R/Beta, and (d) Pt–O/Beta samples.

of literature [49]. After deconvolution, the ratios of $Pt^0/Pt^{2+}$ (area ratios) in the various samples could be estimated, as presented in Table 1. Notably, the $Pt^0$ was predominant on the surface of these samples. However, the $Pt^0/Pt^{2+}$ ratios of the Pt–R samples (5.6 for Beta-H and 3.8 for Beta) were much higher than those (3.5 for Beta-H and 2.5 for Beta) of the Pt–O samples, and the $Pt^0/Pt^{2+}$ ratios of the Beta-H samples (5.6 for Pt–R and 3.5 for Pt–O) were also higher than those (3.8 for Pt–R and 2.5 for Pt–O) of the Beta samples. These results indicate that there are more $Pt^0$ species in the Beta-H samples, which should be attributed to the presence of mesoporosity in the Beta-H samples.

### 3.2. Catalytic performance

#### 3.2.1. Catalytic combustion of toluene over various catalysts

Fig. 6 shows the dependences of the catalytic activities on reaction temperature in the combustion of toluene over Pt–R/Beta-H, Pt–O/Beta-H, Pt–R/Beta, and Pt–O/Beta catalysts. To compare their catalytic activities, $T_5$, $T_{50}$, and $T_{98}$ of toluene were estimated from Fig. 6, as presented in Table 2. Notably, the activities of the reduced catalysts are higher than those of the unreduced catalysts, which are positively related to their proportion of $Pt^0$ species observed from XPS results (Table 1). These results suggest that $Pt^0$ species could be the active centers for the conversion of toluene to $CO_2$ and $H_2O$, in good agreement with those reported previously [32,50].

On the other hand, it is also found that the activities of the mesoporous Beta-H zeolite-supported Pt catalysts are much higher than those of the conventional Beta zeolite-supported Pt catalysts. For example, $T_{98}$ of toluene is only 195 °C over Pt–R/Beta-H, which is about 25 °C lower than that (220 °C) of Pt–R/Beta (Table 2). This phenomenon could be interpreted by the reasons in the following: (i) the Pt–R/Beta-H catalyst has more catalytically active $Pt^0$ species than Pt–R/Beta (Fig. 5 and Table 1), (ii) the Pt particles on mesoporous Beta-H zeolite are smaller than those on the conventional Beta zeolite (Fig. 3), (iii) the mesoporous Beta-H zeolite has better mass transfer than the conventional Beta zeolite.

**Table 1**
XPS results of various samples.

| Catalyst | $Pt4f_{7/2}$ | | $Pt4f_{5/2}$ | | $Pt^0/Pt^{2+}$ (area ratio) |
|---|---|---|---|---|---|
| | BE[a] (eV) | Area | BE[a] (eV) | Area | |
| Pt–R/Beta-H | 70.1 | 740 | 73.4 | 557 | 5.6 |
| | 71.0 | 133 | 74.3 | 100 | |
| Pt–O/Beta-H | 70.1 | 587 | 73.4 | 442 | 3.5 |
| | 71 | 166 | 74.3 | 125 | |
| Pt–R/Beta | 70.1 | 264 | 73.4 | 199 | 3.8 |
| | 71 | 70 | 74.3 | 53 | |
| Pt–O/Beta | 70.1 | 146 | 73.4 | 110 | 2.5 |
| | 71 | 58 | 74.3 | 44 | |

[a] BE: binding energy.

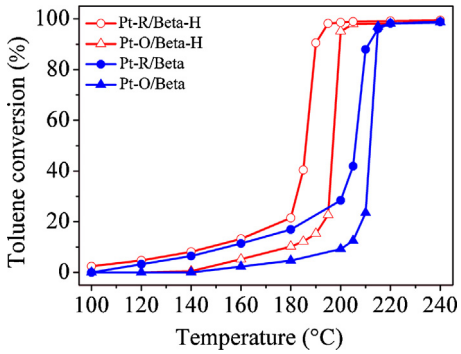


**Fig. 6.** Catalytic combustion of toluene over Pt–R/Beta-H, Pt–O/Beta-H, Pt–R/Beta, and Pt–O/Beta catalysts under the conditions of toluene concentration at 1000 ppm and SV at 60,000 mL/(g h).

**Table 2**
Catalytic data in the combustion of toluene over various catalysts.

| Catalyst | Activities (°C) | | | Ref. |
|---|---|---|---|---|
| | $T_5$ | $T_{50}$ | $T_{98}$ | |
| Pt–R/Beta-H | 121 | 186 | 195 | This work |
| Pt–O/Beta-H | 159 | 197 | 212 | This work |
| Pt–R/Beta | 131 | 206 | 220 | This work |
| Pt–O/Beta | 181 | 212 | 220 | This work |
| Pt–R/Beta-H $SV_1$[a] | 98 | 181 | 189 | This work |
| Pt–R/Beta-H $SV_2$[a] | 142 | 192 | 205 | This work |
| $Pt/Al_2O_3$ $SV_3$[a] $C_1$[b] | | | 260 | [51] |
| Pd(shell)-Au(core)/$TiO_2$ $SV_4$[a] $C_2$[b] | | | 230 | [12] |
| $Pd/mesoZrO_2$ $SV_5$[a] $C_3$[b] | | | 250 | [20] |
| $LaMnO_3$-PP $SV_6$[a] $C_4$[b] | | | 265 | [8] |
| $Mn_{0.5}Ce_{0.5}$ $SV_7$[a] $C_5$[b] | | | 260 | [52] |

[a] Space velocity: $SV_1$ at 30,000 mL/(g h), $SV_2$ at 120,000 mL/(g h), $SV_3$ at 153,000 mL/(g h), $SV_4$ and $SV_5$ at 60,000 mL/(g h), $SV_6$ at 40,000 mL/(g h), and $SV_7$ at 50,000 mL/(g h).
[b] Concentration of toluene: $C_1$ at 225 ppm, $C_2$, $C_3$, and $C_4$ at 1000 ppm, and $C_5$ at 600 ppm.

#### 3.2.2. Catalytic combustion of toluene with various space velocity

Fig. 7 shows the effect of space velocity (SV) on the catalytic activities in the combustion of toluene over Pt–R/Beta-H catalyst.

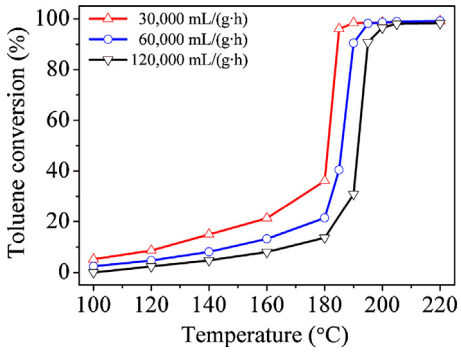


**Fig. 7.** Catalytic combustion of toluene over Pt–R/Beta-H catalyst under the conditions of toluene concentration at 1000 ppm and SV at 30,000 mL/(g h), 60,000 mL/(g h), and 120,000 mL/(g h), respectively.

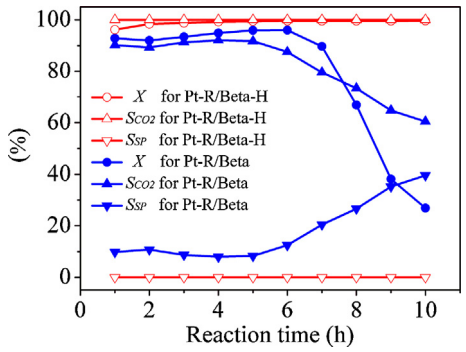


**Fig. 8.** Dependences of activities on reaction time in the catalytic combustion of toluene over Pt–R/Beta-H and Pt–R/Beta catalysts under the conditions of toluene concentration at 1000 ppm, SV at 60,000 mL/(g h), and reaction temperature at 193 °C. $X$, $S_{CO_2}$, and $S_{SP}$ mean toluene conversion, selectivities to $CO_2$ and side products, respectively.

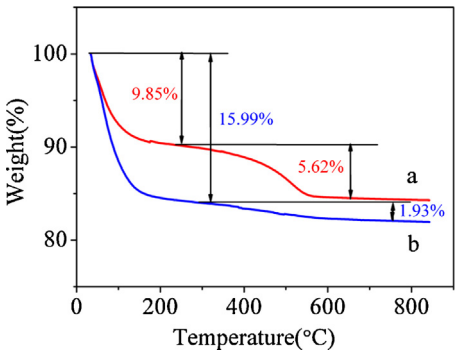


**Fig. 9.** TGA curves of (a) Pt–R/Beta and (b) Pt–R/Beta-H after the catalytic combustion of toluene for 10 h under the conditions of toluene concentration at 1000 ppm, SV at 60,000 mL/(g h), and reaction temperature at 193 °C.

To compare the catalytic activities, $T_5$, $T_{50}$, and $T_{98}$ of toluene were estimated from Fig. 7, as presented in Table 2. When SV is 30,000 mL/(g h), $T_5$, $T_{50}$, and $T_{98}$ values are 98, 181, and 189 °C, respectively. When the SV is increased to 60,000 mL/(g h), $T_5$, $T_{50}$, and $T_{98}$ values are 121, 186, and 195 °C, respectively. Increasing the SV up to 120,000 mL/(g h), $T_5$, $T_{50}$, and $T_{98}$ values are 142, 192, and 205 °C, respectively. These values are much lower than those of reported in literature [8,12,20,51,52], as briefly summarized in Table 2, which indicates that Pt–R/Beta-H is really an active catalyst for the catalytic combustion of VOCs.

### 3.2.3. Catalyst life and coke formation

Fig. 8 shows the dependences of the catalytic activities on reaction time in the combustion of toluene at 193 °C over Pt–R/Beta-H and Pt–R/Beta catalysts. In this reaction, neither CO nor small organic molecules could be detected in the tail gas, $CO_2$ and $H_2O$ are the only products. When the reaction time is less than 5 h, there is no significant drop in the catalytic activities over both Pt–R/Beta-H and Pt–R/Beta catalysts. Both catalysts can get high toluene conversion (over 90%), but their selectivities to $CO_2$ are little distinguishable. For example, at the reaction time of 5 h, Pt–R/Beta-H shows 100% selectivity to $CO_2$ while Pt–R/Beta gives the selectivity at only ca. 90%. When the reaction time increase from 5 to 10 h, the Pt–R/Beta-H catalyst still shows nearly full conversion of toluene and almost 100% selectivity to $CO_2$. In contrast, the Pt–R/Beta catalyst exhibits a significant reduction of toluene conversion and selectivity to $CO_2$ under the same time. For example, when the reaction time reach 10 h, the Pt–R/Beta-H catalyst gives near 100% conversion of toluene and selectivity to $CO_2$, while the Pt–R/Beta catalyst shows 27% toluene conversion and about 60% selectivity to $CO_2$. These results indicate that the Pt–R/Beta-H catalyst has much longer life than Pt–R/Beta, which would be potentially important for practical applications of the catalyst.

Fig. S4 shows the TEM images and Pt particle size distribution of Pt–R/Beta-H and Pt–R/Beta samples after the reaction at 193 °C for 10 h. Notably, the Pt particle sizes (1.8 ± 0.6 nm for Pt–R/Beta-H and 2.4 ± 0.8 nm for Pt–R/Beta) on the used catalysts are very similar to those of the fresh catalysts, suggesting that the Pt particle sintering phenomenon almost does not occur during the reaction. Fig. 9 shows TGA curves of the Pt–R/Beta-H and Pt–R/Beta catalysts after the reaction at 193 °C for 10 h. Both catalysts show two weight losses, giving at below 250 °C and 250–600 °C. The weight loss at below 250 °C is attributed to water desorption, while the weight loss at relatively high temperatures could be assigned to coke formation during the reaction. Comparatively, the weight loss at 250–600 °C of Pt–R/Beta-H (1.93%) is much less than that of Pt–R/Beta (5.62%), indicating that Pt–R/Beta has much stronger coke formation than Pt–R/Beta-H. This phenomenon should be attributed to that Pt–R/Beta-H with mesoporosity is favorable for mass transfer in the catalytic combustion of toluene.

### 3.3. Kinetics

It has been recognized that catalytic combustion of toluene in the presence of excess oxygen is first-order and zero-order kinetics with respect to toluene concentration ($c$) and oxygen concentration, respectively [8,53]. Therefore, the equation is as follows:

$$r = -kc = \left[-A \quad \exp\left(\frac{-E_a}{RT}\right)\right] c \qquad (1)$$

where $r$, $k$, $A$, and $E_a$ stand for the reaction rate [μmol/(g s)], rate constant ($s^{-1}$), pre-exponential factor ($s^{-1}$), and apparent activation energy (kJ/mol), respectively. The $k$ values could be calculated by the reaction rates and reactant conversions.

Fig. 10 shows the Arrhenius plots for the catalytic combustion of toluene at the conversion less than 20% over Pt–R/Beta-H, Pt–O/Beta-H, Pt–R/Beta, and Pt–O/Beta catalysts. The linearity of these plots indicates that the reaction is only in the kinetic controlled region at low temperature where conversion less than 20%, in good agreement with the literature [8,54]. According to the slopes of the Arrhenius plots, we could calculate pre-exponential factors ($A$), apparent activation energies ($E_a$), and correlation coefficients ($R^2$) of the plot ln $k$ versus inverse temperature for the catalytic combustion of toluene, as summarized in Table 3. The results display that the Pt–R/Beta-H catalyst shows the lowest $A$ ($1.19 \times 10^4\ s^{-1}$) and $E_a$ (41 kJ/mol) values. These values are even lower than those reported in the literature [8,55,56], as presented in Table 3, suggesting that Pt–R/Beta-H is really a good catalyst for the catalytic combustion of VOCs.

In addition, Fig. 11 shows the dependences of the turnover frequencies (TOF) on reaction temperature in the catalytic combustion of toluene at conversion less than 20% over Pt–R/Beta-H, Pt–O/Beta-H, Pt–R/Beta, and Pt–O/Beta catalysts. The TOF values over each of the catalysts increased with a rise of reaction temperature. The changing trends of TOF versus reaction temperature over different catalysts are similar to those of toluene conversion versus reaction temperature (Fig. 6). The TOF values over the reduced catalysts are higher than those over the unreduced catalysts, and the TOF values over the mesoporous Beta-H catalysts are higher than those over the conventional Beta catalysts. At the same temperature (160 °C), the TOF values over Pt–R/Beta-H, Pt–O/Beta-H, Pt–R/Beta, and Pt–O/Beta catalysts are summarized in Table 3. The Pt–R/Beta-H catalyst shows the highest TOF value (1.63 $mmol_{toluene}/(mol_{Pt0}\ s)$) at 160 °C, confirming that Pt–R/Beta-H is an efficient catalyst for the catalytic combustion of toluene.

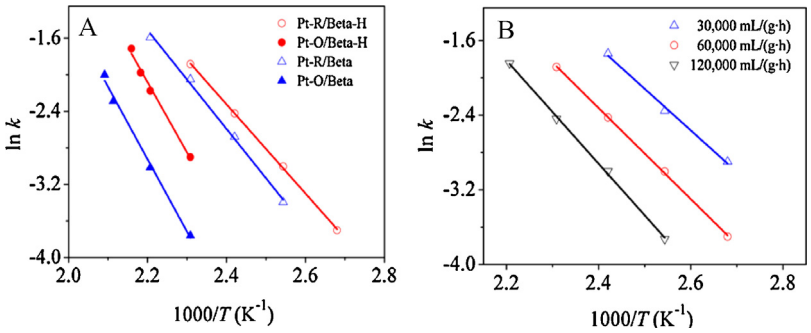


**Fig. 10.** Arrhenius plots for the catalytic combustion of toluene at conversion less than 20% (A) over Pt–R/Beta-H, Pt–O/Beta-H, Pt–R/Beta, and Pt–O/Beta catalysts under the SV at 60,000 mL/(g h) and (B) over Pt–R/Beta-H catalyst under various SV at 30,000 mL/(g h), 60,000 mL/(g h), and 120,000 mL/(g h), respectively.

**Table 3**
Pre-exponential factors ($A$), apparent activation energies ($E_a$), and correlation coefficients ($R^2$) of the plot ln $k$ versus inverse temperature for the catalytic combustion of toluene.

| Catalyst | TOF (160 °C) ($mmol_{toluene}/(mol_{Pt0}\ s)$) | $A$ ($s^{-1}$) | $E_a$ (kJ/mol) | $R^2$ | Ref. |
|---|---|---|---|---|---|
| Pt–R/Beta-H | 1.63 | $1.19 \times 10^4$ | 41 | 0.999 | This work |
| Pt–O/Beta-H | 0.59 | $2.86 \times 10^6$ | 64 | 0.992 | This work |
| Pt–R/Beta | 1.31 | $3.13 \times 10^4$ | 45 | 0.997 | This work |
| Pt–O/Beta | 0.24 | $2.02 \times 10^6$ | 66 | 0.995 | This work |
| 5% Pt/CZB/γ-$Al_2O_3$ | | | 88 | | [55] |
| $LaMnO_3$-PP | | | 57–62 | | [8] |
| CuO–MnO–$CeO_2$/γ-$Al_2O_3$ | | | 70–146 | | [56] |

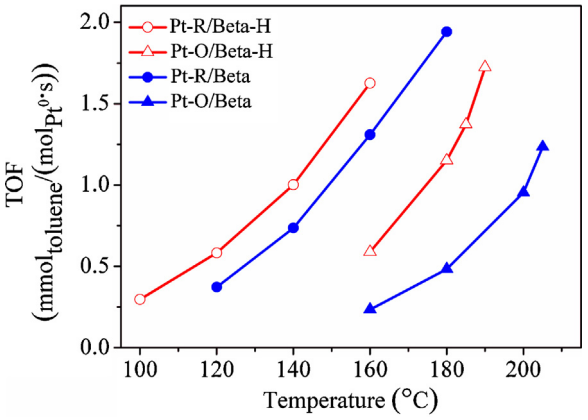


**Fig. 11.** Dependences of the turnover frequencies (TOF) on reaction temperature in the catalytic combustion of toluene at conversion less than 20% over Pt–R/Beta-H, Pt–O/Beta-H, Pt–R/Beta, and Pt–O/Beta catalysts under the conditions of toluene concentration at 1000 ppm and SV at 60,000 mL/(g h).

The difference in $A$, $E_a$ and TOF for various catalysts are also assigned to their distinguishable pore structure, proportion of the active centers, and dispersion of the Pt particles.

## 4. Conclusions

Mesoporous Beta (Beta-H) zeolite-supported Pt catalyst (Pt–R/Beta-H) has been successfully prepared by incipient wetness impregnation of $H_2PtCl_6$ solution with Beta-H zeolite. Very importantly, the Pt–R/Beta-H catalyst is very active, giving superior activities and extraordinary long life, compared with the Pt–R/Beta catalyst prepared by conventional zeolite support. These results could be positively related to the presence of mesoporosity in the Beta-H zeolite, which is favorable for mass transfer and dispersion of Pt particles. The excellent catalytic performance of Pt–R/Beta-H would be potentially important for the catalytic combustion of VOCs in the future.

## Acknowledgments

This work was supported by the National Natural Science Foundation of China (U1162201, 21273197, and 21203165), National High-Tech Research and Development Program of China (2013AA065301), and Science and Technology Innovative Team of Zhejiang Province (No. 2012R10014-02).

## Appendix A. Supplementary data

Supplementary data associated with this article can be found, in the online version, at http://dx.doi.org/10.1016/j.apcatb.2013.03.050.

## References

[1] J.J. Spivey, Industrial & Engineering Chemistry Research 26 (1987) 2165.
[2] P.O. Larsson, A. Andersson, L.R. Wallenberg, B. Svensson, Journal of Catalysis 163 (1996) 279.
[3] W.B. Li, J.X. Wang, H. Gong, Catalysis Today 148 (2009) 81.
[4] C. He, J.R. Li, X.Y. Zhang, L.Q. Yin, J.S. Chen, S.K. Gao, Chemical Engineering Journal 180 (2012) 46.
[5] H.C. Genuino, S. Dharmarathna, E.C. Njagi, M.C. Mei, S.L. Suib, Journal of Physical Chemistry C 116 (2012) 12066.
[6] A.M. Harling, D.J. Glover, J.C. Whitehead, K. Zhang, Environmental Science & Technology 42 (2008) 4546.
[7] Q.G. Huang, S.F. Zuo, R.X. Zhou, Applied Catalysis B 95 (2010) 327.
[8] Y.X. Liu, H.X. Dai, Y.C. Du, J.G. Deng, L. Zhang, Z.X. Zhao, C.T. Au, Journal of Catalysis 287 (2012) 149.
[9] B. de Rivas, R. Lopez-Fonseca, C. Jimenez-Gonzalez, J.I. Gutierrez-Ortiz, Journal of Catalysis 281 (2011) 88.
[10] T. Barakat, J.C. Rooke, H.L. Tidahy, M. Hosseini, R. Cousin, J.F. Lamonier, J.M. Giraudon, G. De Weireld, B.L. Su, S. Siffert, ChemSusChem 4 (2011) 1420.
[11] L.F. Liotta, Applied Catalysis B 100 (2010) 403.
[12] M. Hosseini, T. Barakat, R. Cousin, A. Aboukais, B.L. Su, G. De Weireld, S. Siffert, Applied Catalysis B 111 (2012) 218.
[13] C. He, F.W. Zhang, L. Yue, X.S. Shang, J.S. Chen, Z.P. Hao, Applied Catalysis B 111 (2012) 46.
[14] C.B. Zhang, F.D. Liu, Y.P. Zhai, H. Ariga, N. Yi, Y.C. Liu, K. Asakura, M. Flytzani-Stephanopoulos, H. He, Angewandte Chemie-International Edition 51 (2012) 9628.
[15] C.B. Zhang, H. He, K. Tanaka, Applied Catalysis B 65 (2006) 37.
[16] J.H. Park, B. Kim, C.H. Shin, G. Seo, S.H. Kim, S.B. Hong, Topics in Catalysis 52 (2009) 27.
[17] L. Becker, H. Forster, Applied Catalysis A 153 (1997) 31.

[18] L. Becker, H. Forster, Applied Catalysis B 17 (1998) 43.
[19] H.L. Tidahy, S. Siffert, F. Wyrwalski, J.F. Lamonier, A. Aboukais, Catalysis Today 119 (2007) 317.
[20] H.L. Tidahy, M. Hosseni, S. Siffert, R. Cousin, J.F. Lamonier, A. Aboukais, B.L. Su, J.M. Giraudon, G. Leclercq, Catalysis Today 137 (2008) 335.
[21] A. Corma, Chemical Reviews 95 (1995) 559.
[22] L. Pinard, J. Mijoin, P. Magnoux, M. Guisnet, Comptes Rendus Chimie 8 (2005) 457.
[23] R. Beauchet, P. Magnoux, J. Mijoin, Catalysis Today 124 (2007) 118.
[24] R. Beauchet, J. Mijoin, P. Magnoux, Applied Catalysis B 88 (2009) 106.
[25] J. Tsou, P. Magnoux, M. Guisnet, J.J.M. Orfao, J.L. Figueiredo, Applied Catalysis B 51 (2004) 129.
[26] J. Tsou, P. Magnoux, M. Guisnet, J.J.M. Orfao, J.L. Figueiredo, Applied Catalysis B 57 (2005) 117.
[27] A. Corma, Chemical Reviews 97 (1997) 2373.
[28] M.E. Davis, Nature 417 (2002) 813.
[29] M. Hartmann, Angewandte Chemie-International Edition 43 (2004) 5880.
[30] M. Guisnet, E. Dege, P. Magnoux, Applied Catalysis B 20 (1999) 1.
[31] P. Dege, L. Pinard, P. Magnoux, M. Guisnet, Applied Catalysis B 27 (2000) 17.
[32] P. Dege, L. Pinard, P. Magnoux, M. Guisnet, Comptes Rendus Chimie 4 (2001) 41.
[33] F.S. Xiao, L.F. Wang, C.Y. Yin, K.F. Lin, Y. Di, J.X. Li, R.R. Xu, D.S. Su, R. Schlogl, T. Yokoi, T. Tatsumi, Angewandte Chemie-International Edition 45 (2006) 3090.
[34] W.Q. Fu, L. Zhang, T.D. Tang, Q.P. Ke, S. Wang, J.B. Hu, G.Y. Fang, J.X. Li, F.S. Xiao, Journal of the American Chemical Society 133 (2011) 15346.
[35] T.D. Tang, C.Y. Yin, L.F. Wang, Y.Y. Ji, F.S. Xiao, Journal of Catalysis 249 (2007) 111.
[36] T.D. Tang, C.Y. Yin, L.F. Wang, Y.Y. Ji, F.S. Xiao, Journal of Catalysis 257 (2008) 125.
[37] X.J. Meng, F. Nawaz, F.S. Xiao, Nano Today 4 (2009) 292.
[38] Y.Y. Sun, R. Prins, Angewandte Chemie-International Edition 47 (2008) 8478.
[39] H. Wang, T.J. Pinnavaia, Angewandte Chemie-International Edition 45 (2006) 7603.
[40] M. Choi, H.S. Cho, R. Srivastava, C. Venkatesan, D.H. Choi, R. Ryoo, Nature Materials 5 (2006) 718.
[41] M. Choi, R. Srivastava, R. Ryoo, Chemical Communications (2006) 4380.
[42] R. Srivastava, M. Choi, R. Ryoo, Chemical Communications (2006) 4489.
[43] V.N. Shetti, J. Kim, R. Srivastava, M. Choi, R. Ryoo, Journal of Catalysis 254 (2008) 296.
[44] J. Kim, M. Choi, R. Ryoo, Journal of Catalysis 269 (2010) 219.
[45] K. Cho, H.S. Cho, L.C. de Menorval, R. Ryoo, Chemistry of Materials 21 (2009) 5664.
[46] H.J. Park, H.S. Heo, J.K. Jeon, J. Kim, R. Ryoo, K.E. Jeong, Y.K. Park, Applied Catalysis B 95 (2010) 365.
[47] C. Knapp, A. Obuchi, J.O. Uchisawa, S. Kushiyama, P. Avila, Microporous and Mesoporous Materials 31 (1999) 23.
[48] I. Yordanov, R. Knoerr, V. De Waele, M. Mostafavi, P. Bazin, S. Thomas, M. Rivallan, L. Lakiss, T.H. Metzger, S. Mintova, Journal of Physical Chemistry C 114 (2010) 20974.
[49] L. Xu, X.C. Xu, L.K. Ouyang, X.J. Yang, W. Mao, J.J. Su, Y.F. Han, Journal of Catalysis 287 (2012) 114.
[50] J. Tsou, L. Pinard, P. Magnoux, J.L. Figueiredo, M. Guisnet, Applied Catalysis B 46 (2003) 371.
[51] M. Paulis, H. Peyrard, M. Montes, Journal of Catalysis 199 (2001) 30.
[52] D. Delimaris, T. Ioannides, Applied Catalysis B 84 (2008) 303.
[53] C.T. Wong, A.Z. Abdullah, S. Bhatia, Journal of Hazardous Materials 157 (2008) 480.
[54] F.J. Varela-Gandia, A. Berenguer-Murcia, D. Lozano-Castello, D. Cazorla-Amoros, D.R. Sellick, S.H. Taylor, Applied Catalysis B 129 (2013) 98.
[55] T. Masui, H. Imadzu, N. Matsuyama, N. Imanaka, Journal of Hazardous Materials 176 (2010) 1106.
[56] S.M. Sager, D.I. Kondarides, X.E. Verykios, Applied Catalysis B 103 (2011) 275.